Supporting Information

Tin-Lead Halide Perovskite Solar Cells with a Robust Hole Transport Layer

Chunyan Li[a], Yao Zhang[a], Haiyan Zhao[a], Zhongxun Yu[a], Jixiang Zhang[a], Peng Zhang[ab], Han Chen*[abc]

[a]State Key Laboratory of Metal Matrix Composites, Shanghai Jiao Tong University; Shanghai 200240, China.

[b]Joint Research Center for Clean Energy Materials, Shanghai Jiao Tong University; Shanghai 200240, China.

[c]Innovation Center for Future Materials, Zhangjiang Institute for Advanced Study, Shanghai Jiao Tong University; Shanghai 201203, China.

Corresponding Author

*chen.han@sjtu.edu.cn

Experimental Section

Materials:

Dimethylformamide (DMF, anhydrous 99.8%), dimethyl sulfoxide (DMSO, >99.9%), 1,2-dichlorobenzene (99%), methanol (MeOH, anhydrous 99.8%), ethylene glycol (EG, anhydrous 99.8%), ethyl acetate (EA, anhydrous 99.8%), ethylenediamine (EDA, 99%), SnI_2 (99.99%), SnF_2 (99%), cesium carbonate (99.9%), and glycine hydrochloride (GlyHCl, >99%) are purchased from Sigma-Aldrich. Toluene (99.5%) is obtained from Sinopharm. Lead iodide (PbI_2, 99.99%) and ammonium thiocyanate (NH_4SCN) is purchased from TCI. Formamidinium iodide (FAI) is purchased from Great Cell Solar Materials. C_{60} is bought from Nano-C. Phenethylammonium-chloride (PEACl), phenyl-C_{61}-butyric-acid-methyl-ester (PCBM), and cesium iodide (CsI) are purchased from Xi'an Yuri Solar. Bathocuproine (BCP) is obtained from Wako Chemical. Poly(3,4-ethylenedioxythiophene): poly(styrene sulfonate) (PEDOT:PSS, Clevious P VP AI 4083) was obtained from Heraeus.

Solution preparation:

The CC-incorporated PEDOT:PSS was prepared by mixing refrigerated PEDOT:PSS dispersion (~5 °C) with the aqueous solution of cesium carbonate (50 mg/mL) in the volume ratio of 10: 1. The mixture was filtered through a 0.45 μm PVDF filter before use. For the control PEDOT:PSS HTL, the PEDOT:PSS dispersion was used directly after filtration.

The 1.8 M $Rb_{0.03}Cs_{0.2}FA_{0.77}Pb_{0.5}Sn_{0.5}I_3$ tin-lead perovskite precursor was prepared by dissolving 11.5 mg of RbI, 93.6 mg of CsI, 238.4 mg of FAI, 414.9 mg of PbI_2, 335.3 mg of SnI_2, 14.1 mg of SnF_2, 3 mg of NH_4SCN, 3 mg of GlyHCl, and 1 mg of PEACl in 1 ml of DMF/DMSO (3:1 v/v). The precursor solution was heated at 50 °C overnight and filtered through a 0.22 μm PTFE filter before use.

Device fabrication:

Patterned FTO substrates were sequentially cleaned using detergent, deionized water, acetone, and IPA under ultrasonication for 15 mins. After being dried by nitrogen flow, the substrates were treated with Ar/O_2 (flow ratio 1: 1) plasma for 5 mins. The PEDOT:PSS or CC-PEDOT:PSS dispersion was spin-coated onto the FTO substrates at 6000 rpm for 40 s. After air drying for 20 min, a mixed solvent of MeOH/EG (v/v 30: 1) was applied on the HTL and spin-coated at 6000 rpm for 30 s, followed by annealing at 160 °C for 20 min in air. The substrates were immediately transferred to the N_2-filled glovebox after annealing. The perovskite precursor was spin-coated with a two-step spin-coating program. The first step was at 1000 rpm for 10 s with an acceleration of 200 $rpm \cdot s^{-1}$, and the second step was at 4000 rpm for 50 s with an acceleration of 1000 $rpm \cdot s^{-1}$. 200 μL of EA was dropped 10 s before the end of the spin, and then the substrates were annealed at 100 °C for 10 min. A 5 μg/mL solution of EDA in toluene was applied to the cooled perovskite films by spin coating at 5000 rpm for 30 s, followed by heating at 70 °C for 5 min. The PCBM (5mg/mL in 1,2-dichlorobenzene) is then deposited at 5000 rpm for 30 s, followed by heating at 70 °C for 5 min. C_{60} (18 nm), BCP (7 nm), and Cu (100 nm) in sequential order were thermally evaporated in a vacuum chamber (< 3×10^{-4} Pa).

Film Characterization:

Absorption spectra were recorded by UV-vis-NIR spectrometer (PerkinElmer Lambda 750S). The SEM images were recorded by JSM-7800F (JEOL). The X-ray diffraction (XRD) was conducted using an X-ray diffractometer (Ultima IV) with Cu Kα radiation (λ=1.54 Å) at a scan speed of 5° min^{-1}. X-ray photoelectron spectroscopy (XPS) measurements were performed on a Kratos AXIS Ultra DLD spectrometer by using an Al Ka X-ray source, and the spectra were calibrated with Au $4f_{7/2}$ binding energy (84.0 eV). The Raman spectra were performed by HORIBA LabRAM HR Evolution. Ultraviolet photoelectron spectroscopy (UPS) spectra were

measured with an ESCALAB 250Xi (Thermo Scientific) with a He Iα photon source (21.22 eV). Photoluminescence (PL) spectra and Time-Resolved Photoluminescence (TRPL) spectra were recorded by a steady-state transient fluorescence spectrometer (FLS1000). The Photoluminescence quantum yield (PLQY) was measured by mounting perovskite films in an integrating sphere. Atomic force microscopy (AFM) and conductive-AFM (C-AFM) were conducted on FastScan Bio (Bruker). Spectroscopic ellipsometry was conducted on a Semilab SE-2000 Ellipsometer. The wavelength range was 245.44-1597.01 nm and the angle of incidence was 75 °. The Cauchy model was used for the HTL layer and the Lorentz model was used for the FTO substrate. The ToF-SIMS were based on ION ToF SIMS 5-100 (Germany). A stable Ar ion beam was utilized as the ion beam for in-depth distribution with an analysis area of 100×100 μm^2.

Device Characterization:

J–V curves of the perovskite solar cells were measured with a Keithley 2400 source meter under simulated solar illumination at 100 mW·cm^{-2}, AM 1.5G standard air mass sunlight (Newport, Oriel Class A, 91195A), with anti-reflecting coating layers applied. The simulated light intensity was calibrated by a Si-reference cell. J–V curves were measured by reverse scan (from 1.0 V to -0.1 V) and forward scan (from -0.1 V to 1.0 V) under a constant scan speed of 200 mV·s^{-1} (voltage steps of 10 mV and a delay time of 50 ms). A shadow mask was used to define the active area of the devices as 0.0916 cm^2. External quantum efficiency was obtained using monochromatic incident light of 1×10^{16} photons cm^{-2} in direct current mode (CEP-2000BX, Bunko-Keiki). Space charge limited current (SCLC), dark J-V curves, electrochemical impedance spectroscopy (EIS) and Mott-Schottky curves were collected on an electrochemical analysis instrument (Zahner, Germany). For dark current measurement, the voltage scanned from -0.6 to 1.0 V with the speed of 10 mV·s^{-1} in a dark box. For the Mott-Schottky

measurement, the voltage scanned from -0.1 to 1.0 V with the speed of 10 mV·s^{-1} in a dark box.

The TRPL curves were fitted according to the equation $y = y_0 + A_1 e^{\frac{-t}{\tau_1}} + A_2 e^{\frac{-t}{\tau_2}}$, where A_1 and A_2 are the decay amplitudes, τ_1, and τ_2 are the decay times and y_0 is a constant for the baseline offset. The average lifetime τ_{ave} was calculated according to the equation $\tau_{ave} = \frac{A_1 \tau_1^2 + A_2 \tau_2^2}{A_1 \tau_1 + A_2 \tau_2}$.

The defect density obtained from SCLC measurements was calculated by the equation:

$$N_{defects} = \frac{2\varepsilon\varepsilon_0 V_{TFL}}{eL^2}$$, where ε and ε_0 are the dielectric constant and the vacuum permittivity, respectively, e is the unit charge, and L is the thickness of perovskite film.

The QFLS is calculated based on PLQY values by using the equation:

$$QFLS = k_B T ln(PLQY \times \frac{J_G}{J_{0,rad}})$$, where J_G is the generation current under one illumination (in this case approximated to the J_{sc}), and $J_{0, rad}$ is the radiative recombination current in the dark.

Stability measurements:

For the shelf stability measurement, the unencapsulated devices were stored in the N_2-filled glove box (H_2O, <0.01 ppm; O_2, <0.01 ppm) in the dark. For the thermal stability measurement, the unencapsulated devices were put on a hotplate at 85 °C in an N_2-filled glove box (H_2O, <0.01 ppm; O_2, <0.01 ppm) in dark. For maximum power point tracking, an encapsulated device was operated at the V_{MPP} voltage (0.76 V) under AM1.5G 1-sun illumination, and the ambient temperature was 20-25 °C. The encapsulation was done by glass–glass sealing using UV epoxy resin.

Computational method:

DFT calculations were conducted with the ORCA5.0.3 package[1]. Geometry optimization and single point energy were performed at the M06-2X[2]/Def2-TZVP[3,4] level of theory with D3zero[5] dispersion correction. Structure visualization was conducted by VMD[6].
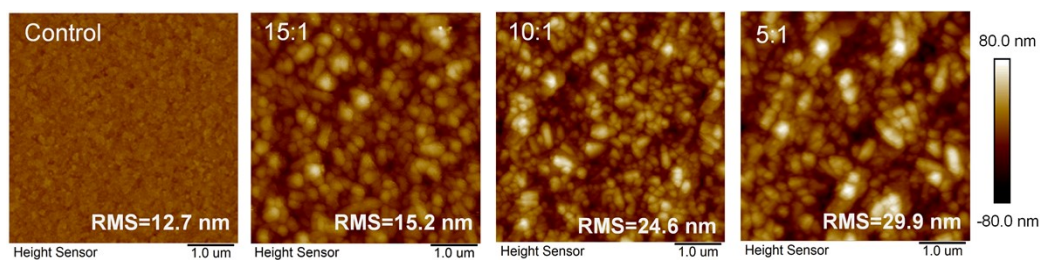

Figure S1. The AFM images of the PEDOT:PSS films with different concentrations of CC.
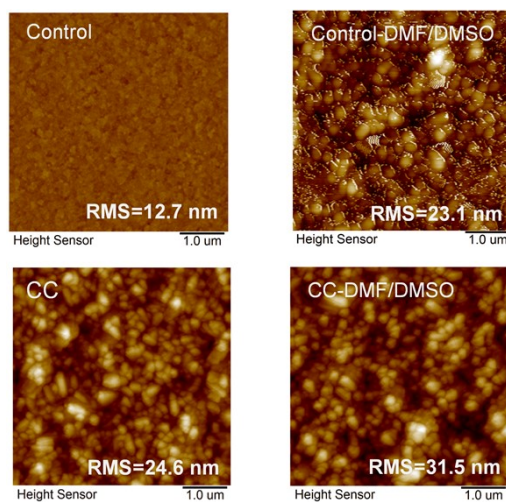

Figure S2. AFM morphologies of the control and CC HTL without and with DMF/DMSO treatment.
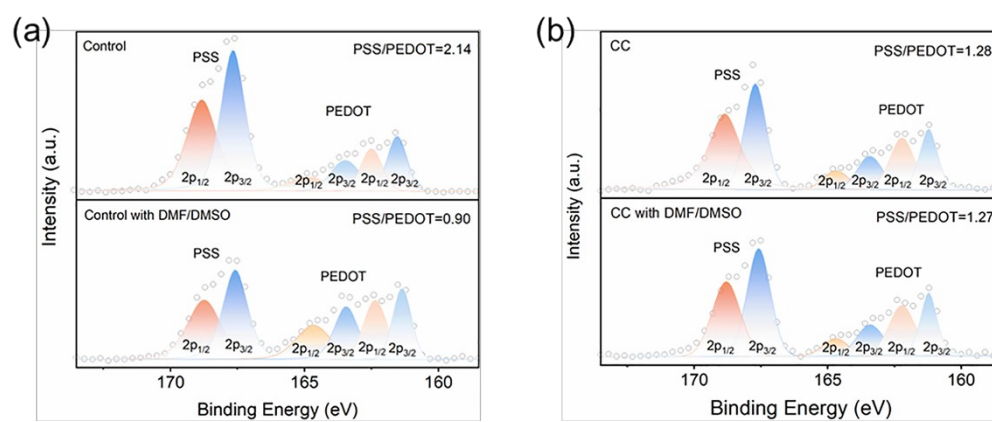
Figure S3. S 2p XRS spectra of the control and CC-PEDOT:PSS with and without DMF/DMSO treatment; see the fitting details in Table S1.
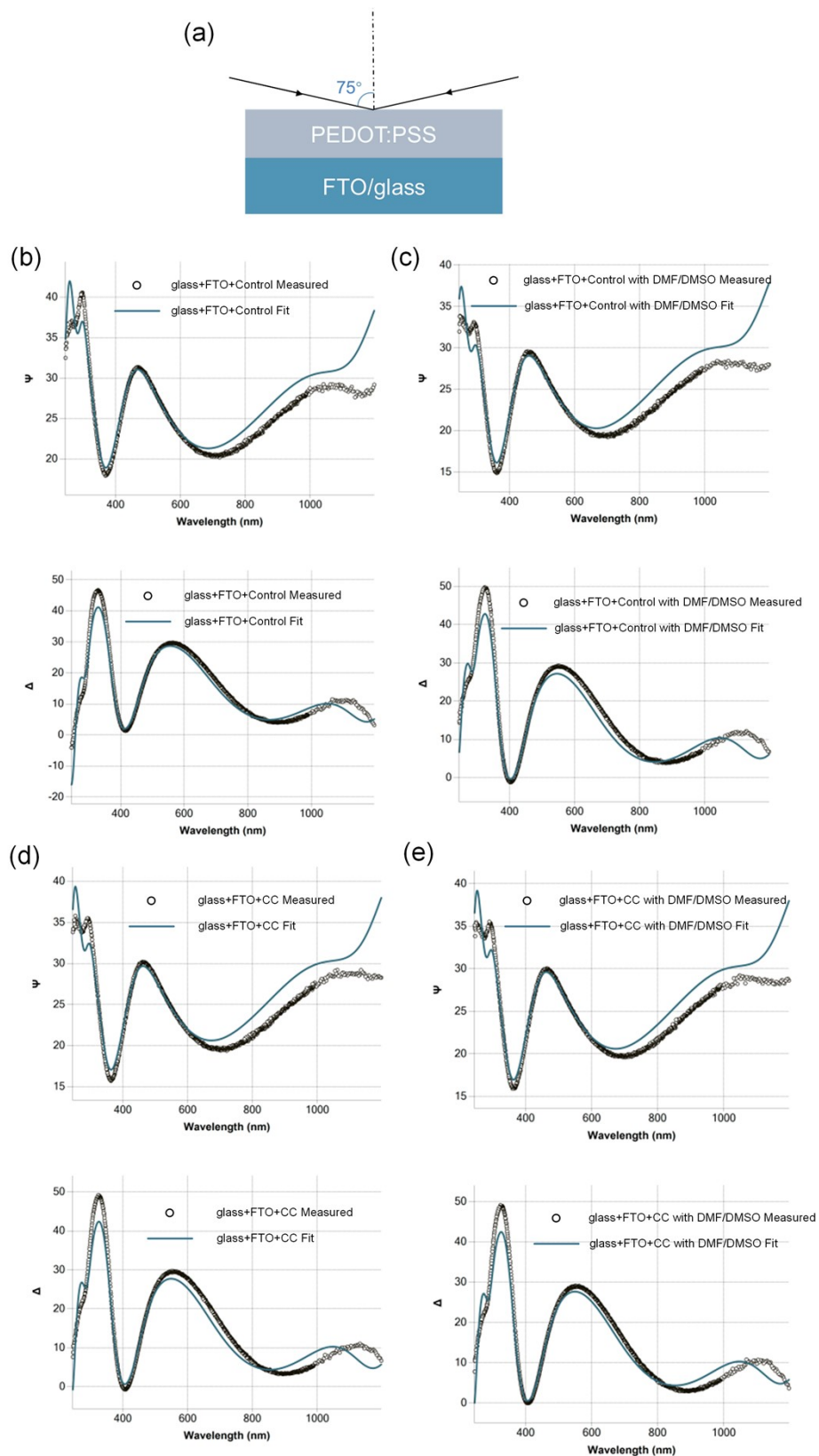
Figure S4. (a) Schematic of the measurements. Experimental and fitted ellipsometry spectra of (b, c) control PEDOT:PSS film and (d, e) CC-PEDOT:PSS film on FTO with and without DMF/DMSO treatment.
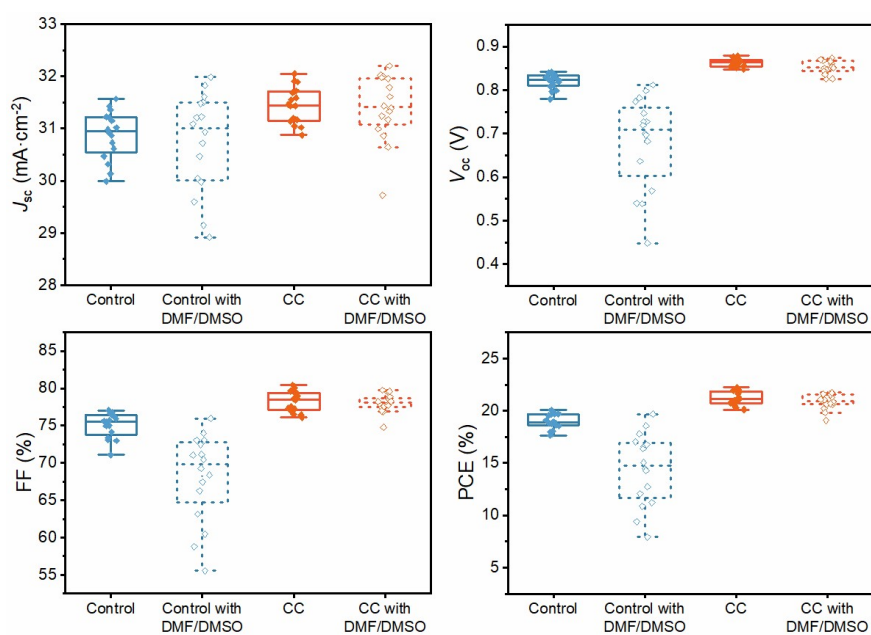
Figure S5. Box charts of PV parameters of devices using control PEDOT:PSS, PEDOT:PSS films with DMF/DMSO washing, CC-doped PEDOT:PSS and CC-doped PEDOT:PSS with DMF/DMSO washing. (These devices were fabricated in one batch)

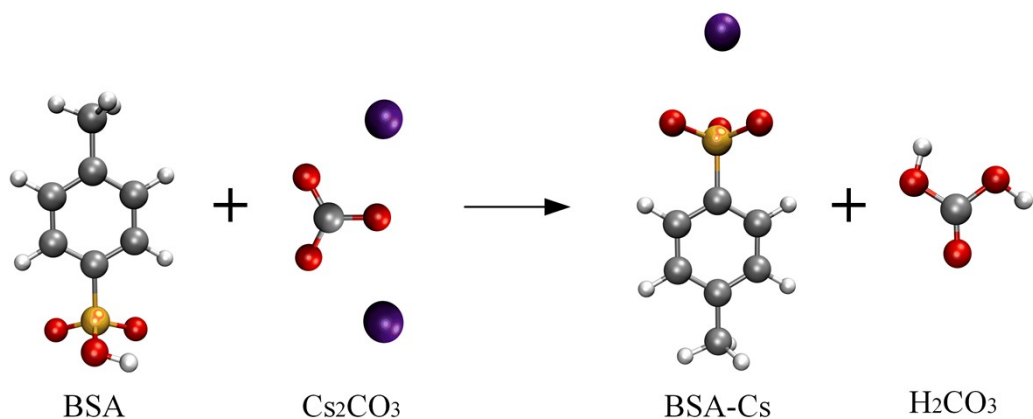Figure S6. PH values of PEDOT: PSS and CC-PEDOT: PSS dispersion.

$$BSA + \tfrac{1}{2}\ Cs_2CO_3 \rightarrow BSA\text{-}Cs + \tfrac{1}{2}\ H_2CO_3 \quad \Delta H = -91.6\ kJ/mol$$
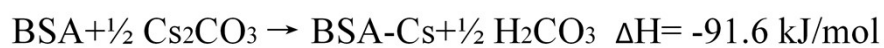
Figure S7. Schematic of the reaction mechanism calculated using DFT. (BSA: benzenesulfonic acid)
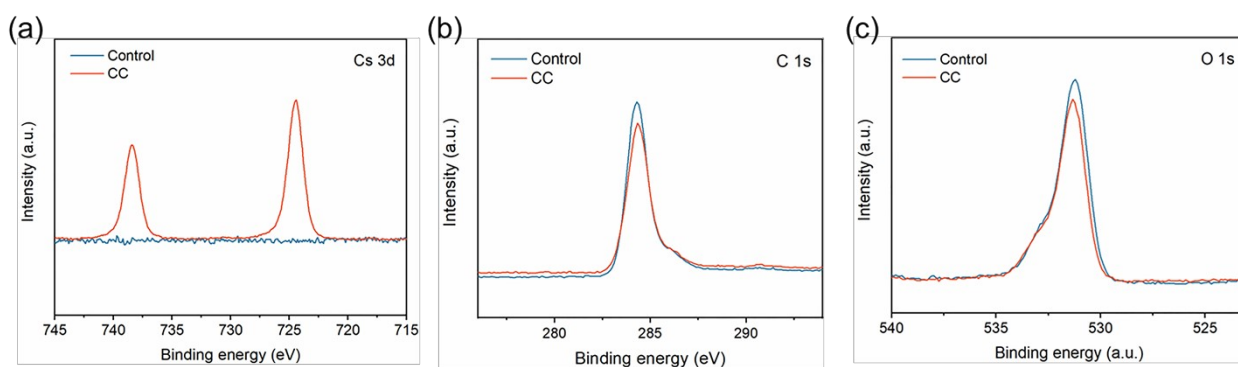
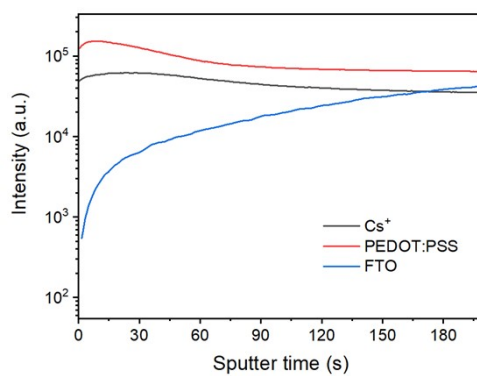Figure S8. Cs 3d, C 1s, and O 1s core levels spectra of the control and CC-PEDOT:PSS layers.

Figure S9. ToF-SIMS depth-profile analysis of the CC-PEDOT:PSS film.
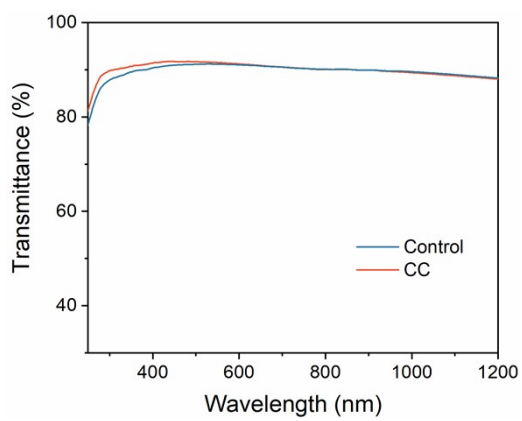

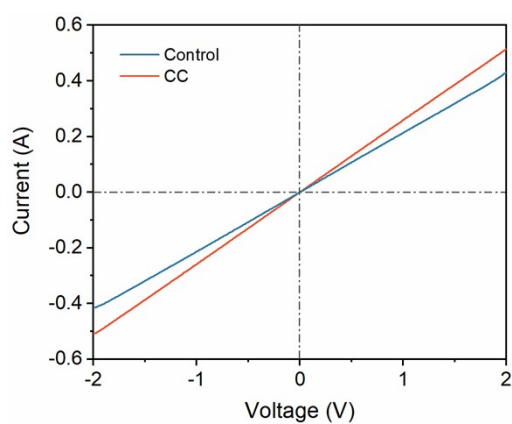Figure S10. Transmittance spectra of control and CC-PEDOT:PSS films on FTO.

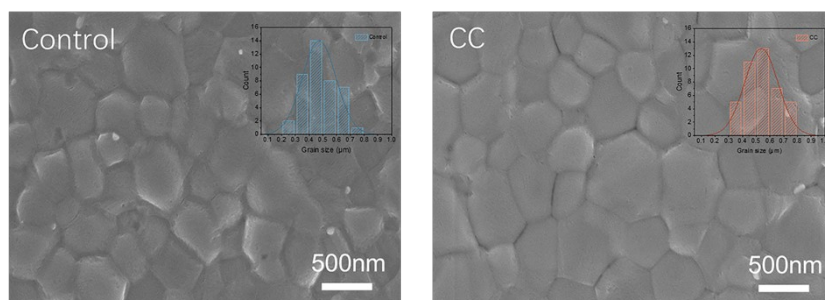Figure S11. Current-voltage characteristics of FTO/PEDOT:PSS/Cu.

Figure S12. Top-view SEM images and grain size distribution (inset) of the perovskite films on the control and CC-PEDOT:PSS layers.
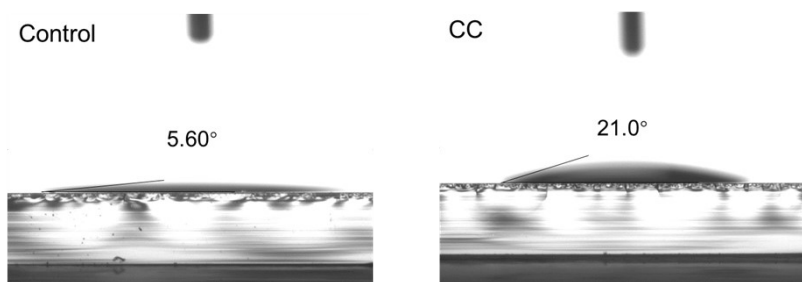
Figure S13. Contact angle images of perovskite precursor on the control and CC-PEDOT:PSS layers.
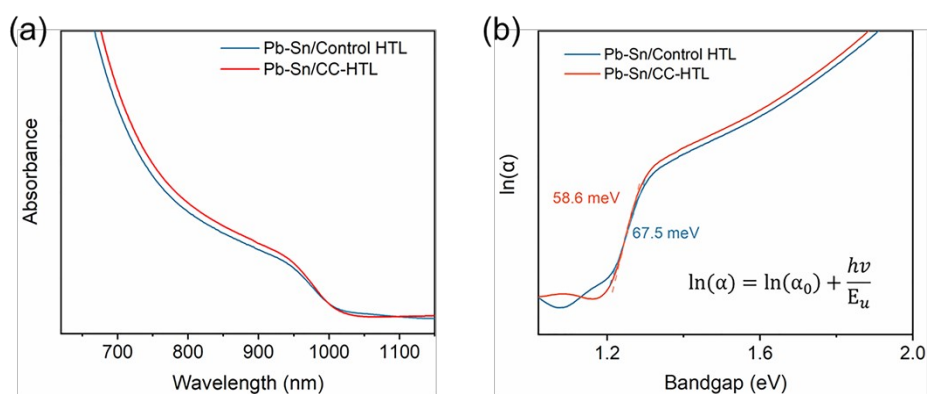

Figure S14. (a) UV–vis absorption spectra and (b) Urbach energy of perovskite film on control and CC-PEDOT:PSS layers.
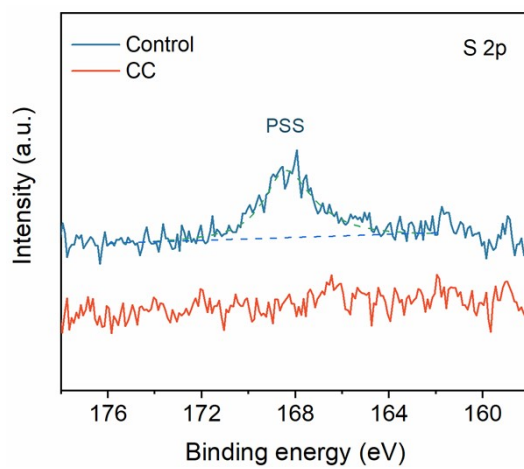
Figure S15. S 2p spectra of the peeled-off perovskite on control and CC-PEDOT:PSS films.
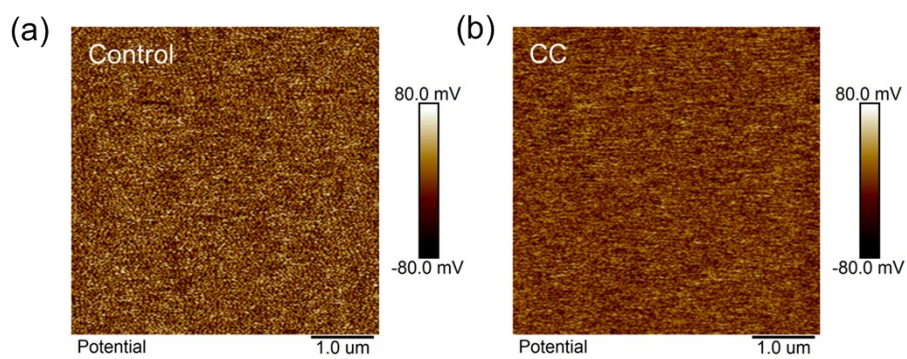

Figure S16. KPFM image of (a) control and (b) CC-PEDOT:PSS films.
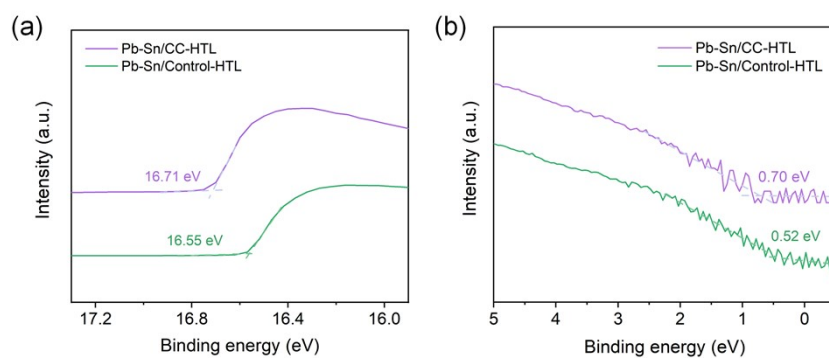
Figure S17. UPS spectra of the Pb-Sn perovskite on the control and CC-PEDOT:PSS layers, (a) cut-off region and (b) valence band edge region.
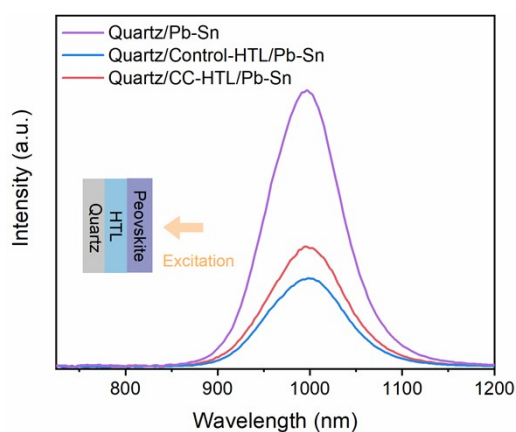
Figure S18. Steady-state PL spectra of neat perovskite film, perovskite/control HTL, and perovskite/CC-HTL were measured from the film side.

Figure S19. Nyquist plot of EIS measurements and the corresponding equivalent circuit model.

Figure S20. Photocurrent density-voltage (*J-V*) curves of perovskite solar cells with various CC solution concentrations.

Report No. 23TR040603

Sample Information

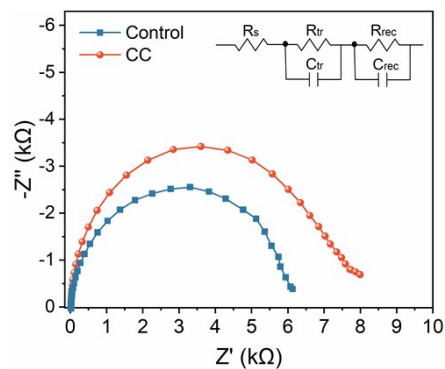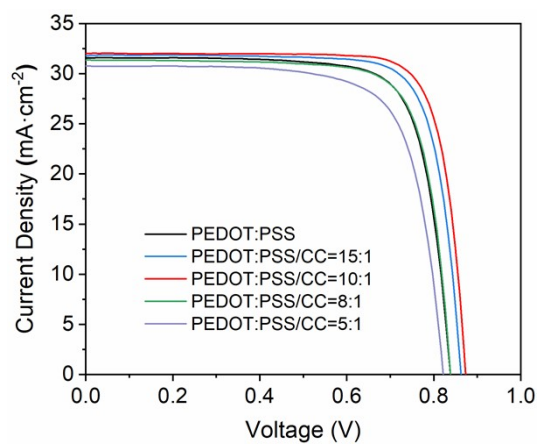| Sample Type	Perovskite photovoltaic cell
Serial No.	2-4#
Lab Internal No.	23040602-1#
Measurement Item	I-V characteristic
Measurement Environment	24.1±2.0°C, 34.3±5.0%R.H

Measurement of I-V characteristic

Reference cell	PVM1121
Reference cell Type	mono-Si, WPVS, calibrated by NREL (Certificate No. ISO 2075)
Calibration Value/Date of Calibration for Reference cell	144.53mA/ Feb. 2023
Measurement Conditions	Standard Test Condition (STC): Spectral Distribution: AM1.5 according to IEC 60904-3 Ed.3, Irradiance: 1000±50W/m², Temperature: 25±2°C
Measurement Equipment/ Date of Calibration	AAA Steady State Solar Simulator (YSS-T155-2M) / July.2022 IV test system (ADCMT 6246) / June. 2022 SR Measurement system (CEP-25ML-CAS) / April.2022 Measuring Microscope (MF-B2017C) / July.2022
Measurement Method	I-V Measurement: Logarithmic sweep in both directions (Isc to Voc and Voc to Isc) during one flash based on IEC 60904-1:2006; Spectral mismatch factor was calculated according to IEC 60904-7 and I-V correction according to IEC 60891.
Measurement Uncertainty	Area: 1.0%(k=2); Isc: 1.9%(k=2); Voc: 1.0%(k=2); Pmax: 2.4%(k=2); Eff: 2.5%(k=2)

Report No. 23TR040603

==== Measurement Results ====

	Forward Scan (Isc to Voc)		Reverse Scan (Voc to Isc)	
Area		9.16 mm²		
Isc	2.911	mA	2.912	mA
Voc	0.866	V	0.870	V
Pmax	2.021	mW	2.042	mW
Ipm	2.770	mA	2.774	mA
Vpm	0.730	V	0.736	V
FF	80.22	%	80.60	%
Eff	22.06	%	22.30	%

- Spectral Mismatch Factor SMM=0.9933.
- Designated illumination area defined by a thin metal mask was measured by a measuring microscope.
- Test results listed in this measurement report refer exclusively to the mentioned test sample.
- The results apply only at the time of the test, and do not imply future performance.
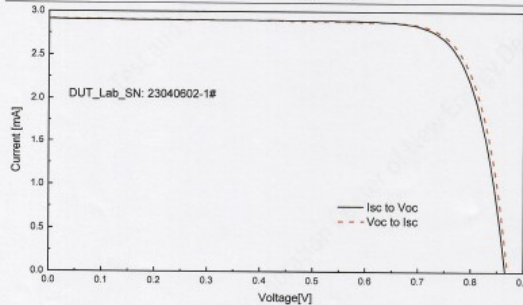
Fig.1 I-V curves of the measured sample

-------End of Report-------

Figure S21. The Certification Report of the champion CCST device at Test and Calibration Center of the New Energy Device and Module, SIMIT, Chinese Academy of Sciences.
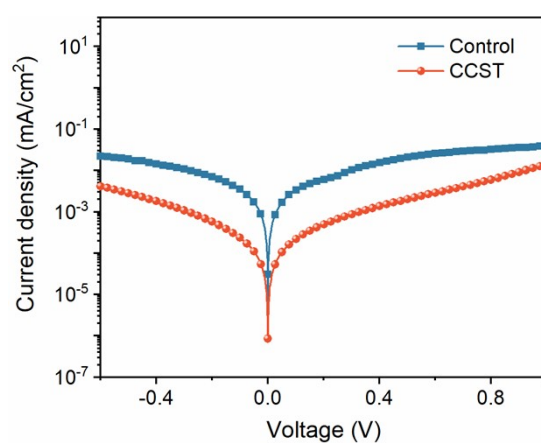
Figure S22. Dark *J-V* curves of control and CCST devices.
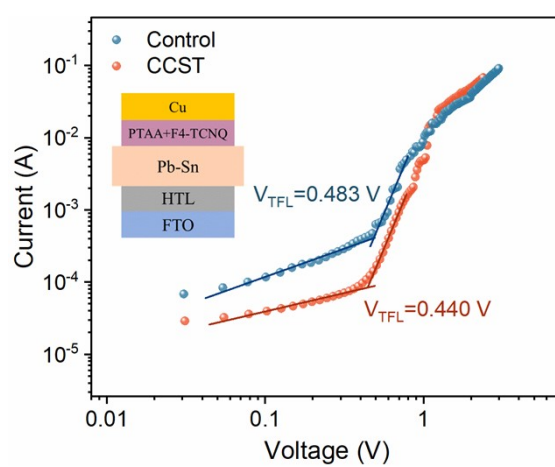
Figure S23. Space charge-limited current (SCLC) measurements of the hole-only devices.

Figure S24. Mott-Schottky plots of control and CCST devices.
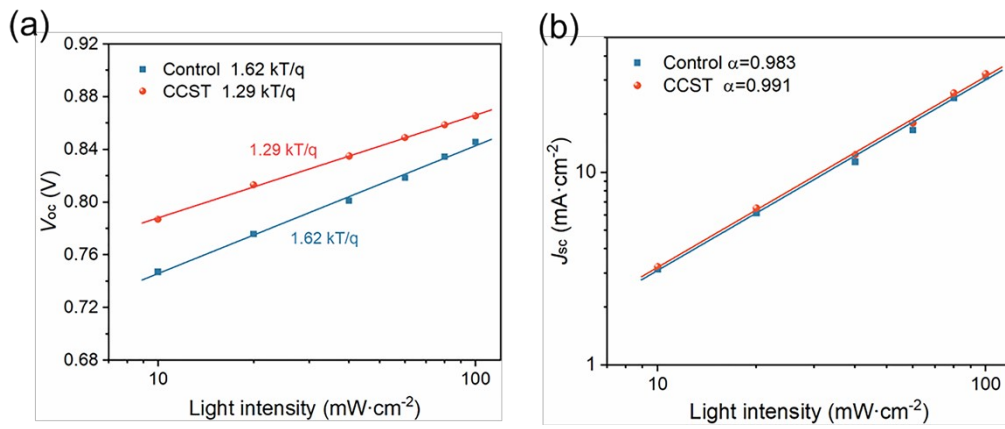
Figure S25. Light intensity dependence of control and CCST perovskite solar cells with (a) V_{oc} versus light intensity and (b) J_{sc} versus light intensity.

Table S1. Detailed information of S 2p XPS spectra for the control and CC- PEDOT:PSS films with and without DMF/DMSO treatment, respectively.
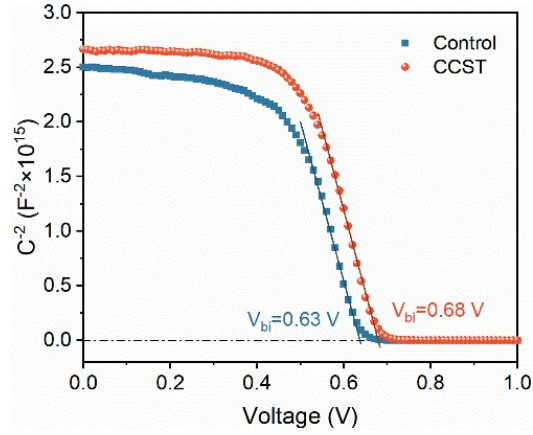
Sample	PSS		PEDOT			
	S $2p_{1/2}$	S 2p3/2	S $2p_{1/2}$	S $2p_{3/2}$	S $2p_{1/2}$	S $2p_{3/2}$
Control	168.85	167.66	164.89	163.48	162.50	161.54
Control with DMF/DMSO	168.74	167.58	164.67	163.44	162.36	161.36
CC	168.82	167.69	164.70	163.43	162.31	161.31
CC with DMF/DMSO	168.76	167.68	164.71	163.41	162.33	161.32

Table S2. Fitting parameters for time-resolved PL decay curves.

Sample	τ_1(ns)	A_1	τ_2(ns)	A_2	$\tau_{average}$(ns)
Pb–Sn/Quartz	150.31	0.356	1178.73	0.525	1096.88
Control HTL	15.54	1.724	139.196	0.292	90.07
CC-HTL	16.58	1.618	232.35	0.219	157.86

Table S3. PLQY and QFLS results of Pb-Sn perovskite film, perovskite/control HTL, and perovskite/CC-HTL half stack.

Sample	PLQY	QFLS (eV)
Pb-Sn/Quartz	0.0617	0.921
Pb-Sn/Control HTL	0.0045	0.850
Pb-Sn/CC-HTL	0.0179	0.889

Table S4. Fitting parameters of electrochemical impedance spectroscopy.

	R_S (Ω)	R_{tr} (Ω)	R_{rec} (Ω)
Control	16.93	1439	5001
CC	18.29	1189	6507

Table S5. Recently reported photovoltaic parameters of MA-free Sn-Pb PSCs.

Device structure	V_{oc}(V)	J_{sc}(mA·cm^{-2})	FF(%)	PCE	Ref
ITO/PEDOT:PSS/Cs$_{0.25}$FA$_{0.75}$Pb$_{0.6}$Sn$_{0.4}$I$_3$/ PCBM/BCP/Ag	0.88	30.78	82.72	22.41	[7]
ITO/neutral PEDOT/Cs$_{0.2}$FA$_{0.8}$Pb$_{0.5}$Sn$_{0.5}$I$_3$/ 1,4-butylenediamine (BDA)/C$_{60}$/BCP/Cu	0.88	32.0	82.0	23.1	[8]
ITO/PEDOT:PSS/Cs$_{0.25}$FA$_{0.75}$Pb$_{0.5}$Sn$_{0.5}$I$_3$/ OH-PEACl/PCBM/BCP/Ag	0.84	30.37	79.18	20.2	[9]
ITO/PEDOT:PSS/ Cs$_{0.3}$FA$_{0.7}$Sn$_{0.3}$Pb$_{0.7}$ I$_3$/C$_{60}$/BCP/Ag	0.787	29.1	79.9	18.3	[10]
Glass/ITO/PEDOT:PSS/ FA$_{0.83}$Cs$_{0.17}$Pb$_{0.5}$Sn$_{0.5}$I$_3$/C$_{60}$/BCP/Ag.	0.795	30.42	76.69	19.12	[11]
ITO/ PEDOT:PSS /FA$_{0.83}$Cs$_{0.135}$Rb$_{0.035}$Sn$_{0.5}$Pb$_{0.5}$I$_3$/ C$_{60}$/BCP/Cu	0.823	31.4	77.8	20.12	[12]
ITO/P3CT-Cs/ FA$_{0.8}$Cs$_{0.2}$Pb$_{0.18}$Sn$_{0.82}$I$_3$/C$_{60}$/TPBi/Ag	0.86	31.55	73.64	20.01	[13]
ITO/PEDOT:PSS/Cs$_{0.25}$FA$_{0.75}$Pb$_{0.6}$Sn$_{0.4}$I$_3$ with D-HLH/PCBM/BCP/Ag	0.88	30.56	80.36	21.6	[14]
ITO/PEDOT:PSS/SnOCl/ Cs$_{0.2}$FA$_{0.8}$Pb$_{0.5}$Sn$_{0.5}$I$_3$/C$_{60}$/BCP/Cu	0.89	32.2	80.9	23.2	[15]
ITO/CzAn/PMMA/Cs$_{0.2}$FA$_{0.8}$Pb$_{0.5}$Sn$_{0.5}$I$_3$/C$_{60}$/ BCP/Cu	0.87	32.64	79.62	22.6	[16]
ITO/PEDOT:PSS/FA$_{0.8}$Cs$_{0.2}$Pb$_{0.5}$Sn$_{0.5}$I$_3$/C$_{60}$/ BCP/Cu	0.86	31.5	78.1	21.2	[17]
ITO/resin particle/neutral PEDOT /Cs$_{0.2}$FA$_{0.8}$Pb$_{0.5}$Sn$_{0.5}$I$_3$/C$_{60}$/SnO$_2$/ITO	0.85	30.2	76.4	19.6	[18]
FTO/CC-PEDOT:PSS/ Rb$_{0.03}$Cs$_{0.2}$FA$_{0.77}$Pb$_{0.5}$Sn$_{0.5}$I$_3$/PCBM/C$_{60}$/BCP/Cu	0.885 / 0.870	32.25 / 31.79	81.22 / 80.60	23.18 / 22.30[*]	This work

* Certified efficiency

References:

1. F. Neese, F. Wennmohs, U. Becker and C. Riplinger, *The Journal of Chemical Physics*, 2020, **152**, 224108.

2. Y. Zhao and D. G. Truhlar, *Theoretical Chemistry Accounts*, 2008, **120**, 215-241.

3. F. Weigend and R. Ahlrichs, *Physical Chemistry Chemical Physics*, 2005, **7**, 3297.

4. F. Weigend, *Physical Chemistry Chemical Physics*, 2006, **8**, 1057.

5. S. Grimme, J. Antony, S. Ehrlich and H. Krieg, *The Journal of Chemical Physics*, 2010, **132**, 154104.

6. W. Humphrey, A. Dalke and K. Schulten, *J. Mol. Graph.*, 1996, **14**, 33-38.

7. Z. Zhang, J. Liang, J. Wang, Y. Zheng, X. Wu, C. Tian, A. Sun, Y. Huang, Z. Zhou and Y. Yang, *Adv. Energy Mater.*, 2023, **13**, 2300181.

8. J. Wang, M. A. Uddin, B. Chen, X. Ying, Z. Ni, Y. Zhou, M. Li, M. Wang, Z. Yu and J. Huang, *Adv. Energy Mater.*, 2023, **13**, 2204115.

9. C. Tian, Z. Zhang, A. Sun, J. Liang, Y. Zheng, X. Wu, Y. Liu, C. Tang and C.-C. Chen, *Nano Energy*, 2023, **116**, 108848.

10. J. Tong, J. Gong, M. Hu, S. K. Yadavalli, Z. Dai, F. Zhang, C. Xiao, J. Hao, M. Yang and M. A. Anderson, *Matter*, 2021, **4**, 1365-1376.

11. T. Jiang, X. Xu, Z. Lan, Z. Chen, X. Chen, T. Liu, S. Huang and Y. M. Yang, *Nano Energy*, 2022, **101**, 107596.

12. F. Yang, R. W. MacQueen, D. Menzel, A. Musiienko, A. Al-Ashouri, J. Thiesbrummel, S. Shah, K. Prashanthan, D. Abou-Ras and L. Korte, *Adv. Energy Mater.*, 2023, 2204339.

13. W. Zhang, X. Li, S. Fu, X. Zhao, X. Feng and J. Fang, *Joule*, 2021, **5**, 2904-2914.

14. Z. Zhang, J. Liang, J. Wang, Y. Zheng, X. Wu, C. Tian, A. Sun, Z. Chen and C.-C. Chen, *Nano-Micro Lett*, 2022, **14**, 165.

15. Z. Yu, J. Wang, B. Chen, M. A. Uddin, Z. Ni, G. Yang and J. Huang, *Adv. Mater.*, 2022, **34**, 2205769.

16.   J. Wang, Z. Yu, D. D. Astridge, Z. Ni, L. Zhao, B. Chen, M. Wang, Y. Zhou, G. Yang and X. Dai, *ACS Energy Lett.*, 2022, **7**, 3353-3361.

17.   Z. Yu, X. Chen, S. P. Harvey, Z. Ni, B. Chen, S. Chen, C. Yao, X. Xiao, S. Xu and G. Yang, *Adv. Mater.*, 2022, **34**, 2110351.

18.   B. Chen, Z. Yu, A. Onno, Z. Yu, S. Chen, J. Wang, Z. C. Holman and J. Huang, *Science Advances*, 2022, **8**.